Revealing the effect of water vapor pressure on the kinetics of thermal decomposition of magnesium hydroxide

Satoki Kodani,[1] Shun Iwasaki,[1] Loïc Favergeon,[2] and Nobuyoshi Koga[1,*]

[1]Chemistry Laboratory, Department of Science Education, Graduate School of Education, Hiroshima University, 1-1-1 Kagamiyama, Higashi-Hiroshima 739-8524, Japan.

[2]Mines Saint-Etienne, University of Lyon, CNRS, UMR 5307 LGF, Centre SPIN, F-42023 Saint-Etienne, France.

Contents

* Corresponding author. E-mail: nkoga@hiroshima-u.ac.jp

S1. Instrumental setup

Measurements of the mass-loss curves under controlled $p(H_2O)$ conditions were performed using a controlled humidity TG–DTA system (HUM-TG, Thermoplus 2, Rigaku).[84] Figure S1 shows the system comprises a horizontally configured thermobalance (TG-8120, Thermoplus 2, Rigaku) with an electric furnace surrounded by a water jacket, a water circulator with a temperature controller (F-25, Julabo), a humidity controller (HUM-1, Rigaku), and a transfer tube with a temperature controller between the humidity controller and the thermobalance, and a dry N_2 gas supply line connected from a N_2 gas cylinder equipped with a pressure regulator.

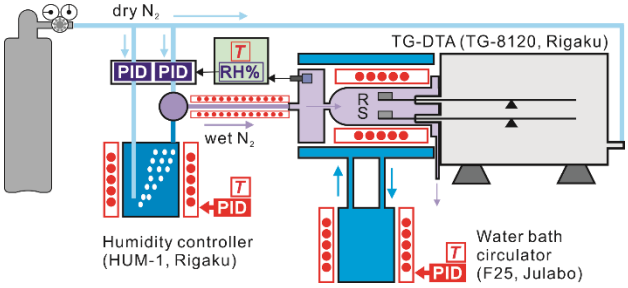

Figure S1. Overview of the controlled humidity TG–DTA system (HUM-TG, Thermoplus 2, Rigaku).

Before measurement, the electric furnace of the thermobalance and an anterior chamber connected to the furnace tube were warmed up by circulating water of controlled constant temperature ranging from 293–353 K. A purge gas of dry N_2 flowed through at a rate of 50 cm^3 min^{-1} from the back of the balance system. After the sample was set on the sample holder in the thermobalance, the sample was heated to 353 K at a heating rate of 5 K min^{-1} under a stream of dry N_2 gas at 400 cm^3 min^{-1} introduced from the forefront of the furnace via the anterior chamber and held at the programmed temperature for 30 min. Immediately after the sample reached the programmed temperature, the dry N_2 gas from the front of the furnace was switched to wet N_2 gas at a controlled $p(H_2O)$ value.

The wet N_2 gas was generated in the humidity controller by bubbling N_2 gas in a temperature-controlled water bath. The wet and dry N_2 gases were mixed and transferred in the anterior chamber of the furnace at a rate of 400 cm^3 min^{-1} via a transfer tube heated at a temperature ranging from 308–373 K. In the anterior chamber, the relative humidity and temperature of the wet N_2 gas were continuously measured, with the relative humidity signal returned to the humidity controller for the control of flowrates of the wet and dry N_2 gases to be mixed, so as to regulate the relative humidity in the anterior chamber to be the programmed value. The $p(H_2O)$ value of the wet N_2 gas in the anterior chamber was calculated using the temperature and relative humidity values. The wet N_2 gas with the controlled $p(H_2O)$ value was passed over the sample and ejected through the part of the furnace linked to the balance room, together with the dry N_2 gas that purged the balance room.

After stabilized the measurement system under a stream of wet N_2 gas with the controlled $p(H_2O)$ value for 30 min, the mass-loss curves for the thermal decomposition of the $Mg(OH)_2$ sample were obtained at the set $p(H_2O)$ value under isothermal and linear nonisothermal conditions. Typical records of the mass-change measurements are depicted in Figure S2.

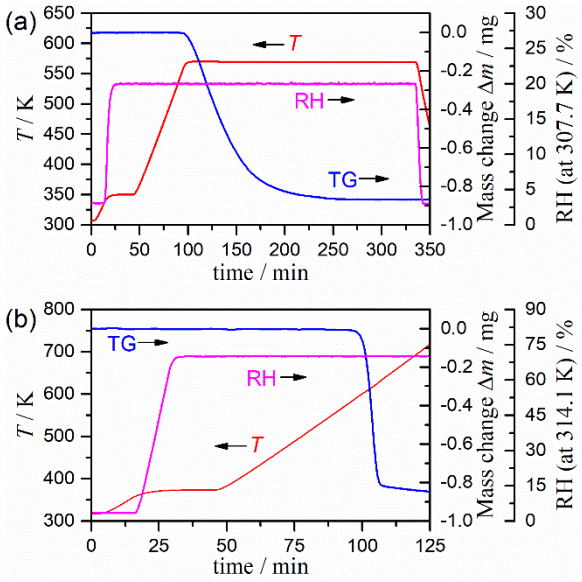

Figure S2. Typical records of the mass-change measurements for the thermal decomposition of the $Mg(OH)_2$ sample under a stream of wet N_2 gas with controlled $p(H_2O)$: (a) isothermal and (b) linear nonisothermal conditions.

The TG–DTA instrument was initially calibrated in relation to the changes in mass values and the measured sample temperature. The changes in mass values were calibrated at room temperature and ambient atmosphere during opening of the furnace by the addition/removal of a 10 mg standard weight to/from the sample holder. Subsequently, the TG–DTA curves for the thermal decomposition of approximately 10 mg of a calcium oxalate monohydrate sample (>99.9985%, Alfa Aesar) were recorded at a β of 5 K min^{-1} under a stream of wet N_2 gas at a controlled $p(H_2O)$ of approximately 5.0 kPa (flowrate: 400 cm^3 min^{-1}). The reliability of the changes in mass values recorded under a stream of wet N_2 gas were confirmed by comparing the recorded changes in mass values with expected values for the following three reaction steps:

$CaC_2O_4 \cdot H_2O \rightarrow CaC_2O_4 + H_2O$ (−12.3%)
$CaC_2O_4 \rightarrow CaCO_3 + CO$ (−19.2%)
$CaCO_3 \rightarrow CaO + CO_2$ (−30.1%)

TG–DTA measurements for various pure metal samples including In, Sn, Pb, Zn, Al, and Ag (>99.99%, Nilaco) were conducted under identical conditions as those for the thermal decomposition of $CaC_2O_4 \cdot H_2O$. The measured onset temperatures of the DTA

endothermic peaks for the melting of these pure metals were calibrated with reference to values in the literature for those melting points. In addition, the calibrated temperature was confirmed as applicable to the measurements under a stream of wet N_2 gas with different $p(H_2O)$ values through measurements of the DTA endothermic peak for melting of In under various $p(H_2O)$ conditions.

S2. Formal kinetic analysis without considering the effect of water vapor pressure

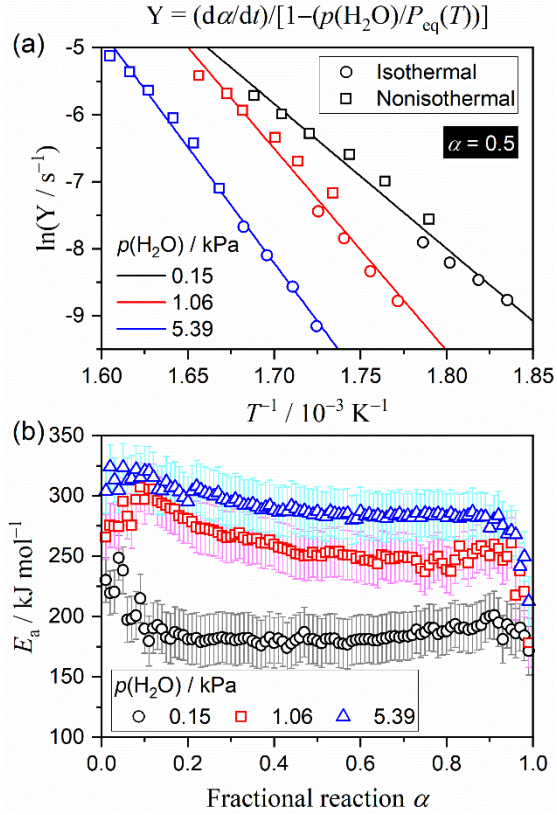

Figure S3. Results of the modified Friedman plot with $a(p(H_2O), P_{eq}(T))$ in eqn (9) applied to the thermal decomposition of the $Mg(OH)_2$ sample at different $p(H_2O)$ values: (a) modified Friedman plots at α = 0.5 and (b) E_a values at various α.

Table S1. The average E_a values for $0.1 \le \alpha \le 0.9$, determined by the modified Friedman plot with $a(p(H_2O), P_{eq}(T))$ in eqn (9)

$p(H_2O)$ / kPa	E_a / kJ mol^{-1}	$-\gamma$ [a]
0.15	183.7 ± 9.8	0.9887 ± 0.0019
1.06	259.8 ± 17.7	0.9817 ± 0.0100
5.39	290.5 ± 8.6	0.9966 ± 0.0007

[a] Average value of the correlation coefficient of the linear regression analysis for the modified Friedman plot at various α values in $0.1 \le \alpha \le 0.9$.

S3. Formal kinetic analysis with considering the effect of water vapor pressure

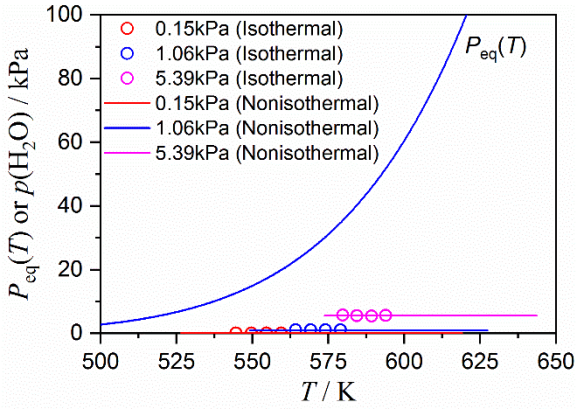

Figure S4. Equilibrium water vapor pressure for thermal decomposition of $Mg(OH)_2$ calculated using MALT2[96,97] and the applied $p(H_2O)$ values for recording the kinetic data.

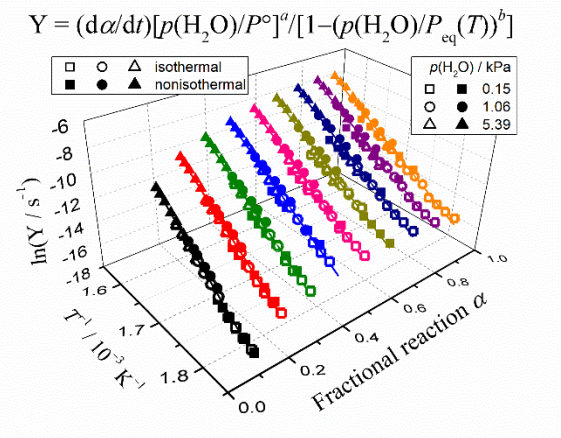

Figure S5. Modified Friedman plots with the AF in eqn (2) applied universally to the kinetic curves derived at different temperature and $p(H_2O)$ conditions.

S4. Universal kinetic modeling of the physico-geometrical consecutive process at different water vapor pressures

The physico-geometrical consecutive SR–PBR(n) models assume the first-order kinetic behavior on the surfaces of reactant particles in the sample assemblage and subsequent n-dimensional shrinkage of the reaction interface in each reactant particles controlled by chemical reaction. Each kinetic curve recorded isothermally at different temperatures and under different $p(H_2O)$ values were separately subjected to the kinetic calculation based on the SR–PBR(n) models listed in Table S2. Before fitting the experimental kinetic curve by that calculated according to the kinetic equations, the initial value for $k_{PBR(n)}$ was calculated with reference to the kinetic parameters determined preliminary using the isoconversional kinetic analysis without considering the effect of $p(H_2O)$. After the initial value of $k_{PBR(n)}$ was set in the kinetic equations, the order of k_{SR} initial value was determined by graphically comparing the experimental and calculated kinetic curves. Then, the simultaneous optimizations of $k_{PBR(n)}$ and k_{SR} via nonlinear least squares analysis were run to minimize the squares sum, F.

$$F = \sum_{j=1}^{M} \left[\left(\frac{\mathrm{d}\alpha}{\mathrm{d}t}\right)_{\mathrm{exp},j} - \left(\frac{\mathrm{d}\alpha}{\mathrm{d}t}\right)_{\mathrm{cal},j} \right]^2 \tag{S1}$$

where M is the number of data points in each kinetic curve. The most appropriate kinetic model was selected by comparing the statistical significances of the fittings obtained using different kinetic models in Table S2. Irrespective of the kinetic curve, the experimental kinetic curves were best described by the SR–PBR(3) model. Table S3 lists the optimized k_{SR} and $k_{PBR(n)}$ values for the reaction at different temperatures and $p(H_2O)$ values. The universal kinetic analysis of each physico-geometrical reaction step over different temperature and $p(H_2O)$ conditions are demonstrated using the optimized k_{SR} and $k_{PBR(n)}$ values and described in the main article.

Table S2. Differential kinetic equations for the SR–PBR(n) model

n	$\frac{\mathrm{d}\alpha}{\mathrm{d}t} =$
1	a) $t \le 1/k_{PBR(1)}$: $k_{PBR(1)}[1 - \exp(-k_{SR}t)]$
	b) $t \ge 1/k_{PBR(1)}$: $k_{PBR(1)}\exp(-k_{SR}t)\left[\exp\left(\frac{k_{SR}}{k_{PBR(1)}}\right) - 1\right]$
2	a) $t \le 1/k_{PBR(2)}$: $-2k_{PBR(2)}\left[\left(1 + \frac{k_{PBR(2)}}{k_{SR}}\right)\exp(-k_{SR}t) + k_{PBR(2)}t - \left(1 + \frac{k_{PBR(2)}}{k_{SR}}\right)\right]$
	b) $t \ge 1/k_{PBR(2)}$: $-2k_{PBR(2)}\exp(-k_{SR}t)\left[1 + \frac{k_{PBR(2)}}{k_{SR}} - \frac{k_{PBR(2)}}{k_{SR}}\exp\left(\frac{k_{SR}}{k_{PBR(2)}}\right)\right]$
3	a) $t \le 1/k_{PBR(3)}$: $-3k_{PBR(3)}\left[\left(1 + 2\frac{k_{PBR(3)}}{k_{SR}} + 2\left(\frac{k_{PBR(3)}}{k_{SR}}\right)^2\right)\exp(-k_{SR}t) - \left(-k_{PBR(3)}t\right)^2 + 2k_{PBR(3)}\left(\frac{k_{PBR(3)}}{k_{SR}} + 1\right)t - \left(1 + 2\frac{k_{PBR(3)}}{k_{SR}} + 2\left(\frac{k_{PBR(3)}}{k_{SR}}\right)^2\right)\right]$
	b) $t \ge 1/k_{PBR(3)}$: $3k_{PBR(3)}\exp(-k_{SR}t)\left[2\left(\frac{k_{PBR(3)}}{k_{SR}}\right)^2\left(\exp\left(\frac{k_{SR}}{k_{PBR(3)}}\right) - 1\right) - \left(1 + 2\frac{k_{PBR(3)}}{k_{SR}}\right)\right]$

Table S3. Optimized k_{SR} and $k_{PBR(3)}$ values for thermal decomposition of the $Mg(OH)_2$ sample at different temperature and $p(H_2O)$ conditions

$p(H_2O)$ / kPa	T / K	k_{SR} / s^{-1}	$k_{PBR(3)}$ / s^{-1}	$R^{2,a}$	
				differential	integral
0.15	544.6	2.70×10^{-4}	8.31×10^{-4}	0.9871	0.9956
	549.7	3.75×10^{-4}	1.20×10^{-3}	0.9973	0.9978
	554.7	5.03×10^{-4}	4.85×10^{-3}	0.9957	0.9998
	559.5	6.67×10^{-4}	4.94×10^{-3}	0.9972	0.9998
1.06	564.3	3.12×10^{-4}	2.14×10^{-4}	0.9529	0.9982
	569.2	4.70×10^{-4}	3.87×10^{-4}	0.9926	0.9984
	574.0	7.32×10^{-4}	6.50×10^{-4}	0.9906	0.9986
	579.0	1.10×10^{-3}	1.14×10^{-3}	0.9959	0.9985
5.39	579.8	3.82×10^{-4}	8.70×10^{-5}	0.9826	0.9996
	584.4	5.03×10^{-4}	1.55×10^{-4}	0.9899	0.9999
	589.2	6.69×10^{-4}	3.45×10^{-4}	0.9966	0.9998
	594.0	1.11×10^{-3}	4.29×10^{-4}	0.9973	0.9998

[a] Determination coefficient of the nonlinear least squares analysis.

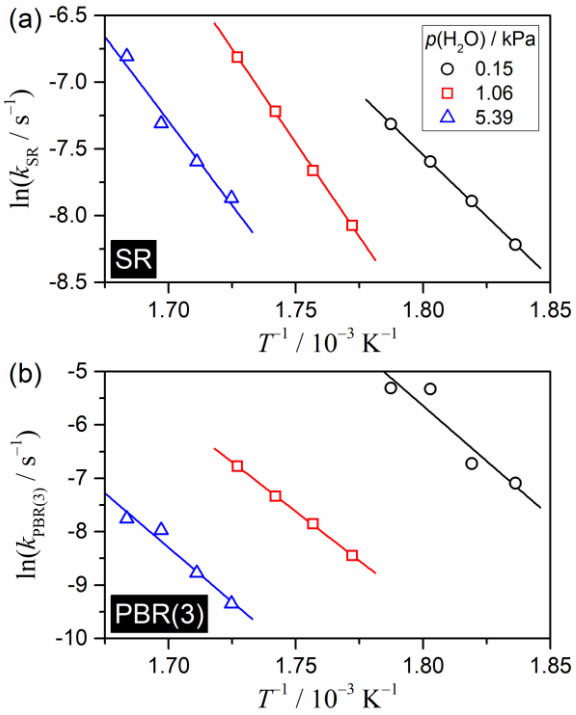

Figure S6. Conventional Arrhenius plot applied to the optimized rate constants for each reaction step: (a) SR and (b) PBR(3).

Table S4. Apparent Arrhenius parameters for each reaction step determined using the conventional Arrhenius plot without considering the effect of $p(H_2O)$

Reaction step	$p(H_2O)$ / kPa	E_a / kJ mol^{-1}	ln(A / s^{-1})	$-\gamma$ [a]
SR	0.15	153.4 ± 1.5	25.7 ± 1.5	0.9999
	1.06	233.9 ± 3.5	41.8 ± 0.8	0.9998
	5.39	210.0 ± 24.4	35.7 ± 5.0	0.9868
PBR(3)	0.15	344.3 ± 89.9	68.9 ± 19.6	0.9382
	1.06	307.2 ± 3.9	57.0 ± 0.9	0.9998
	5.39	338.5 ± 47.7	60.9 ± 9.8	0.9808

[a] Correlation coefficient of the linear regression analysis.

S5. Comparison with the reactions of other metal hydroxides

Table S5. Summary of the previously reported kinetic results obtained by the modified Arrhenius plots with the AF in eqn (2) for each reaction step, based on the IP–SR–PBR(n) model for the thermal decompositions of $Ca(OH)_2$ and $Cu(OH)_2$ over a range of temperature and $p(H_2O)$ conditions

reaction	step	AF in eqn (2)		E_a / kJ mol^{-1}	ln(A / s^{-1})	$-\gamma$ [a]	ref.
		a	b				
$Ca(OH)_2$	IP	4.75	1.86	736.8 ± 15.4	74.8 ± 2.6	0.9965	9
→ $CaO + H_2O$	SR	3.79	1.65	610.4 ± 11.4	66.5 ± 3.0	0.9972	
	PBR(2)	3.36	1.91	539.7 ± 14.0	52.7 ± 2.5	0.9947	
$Cu(OH)_2$	IP	0.41	12.67	242.4 ± 13.0	65.8 ± 4.0	0.9819	10
→ $CuO + H_2O$	SR	0.41	16.28	164.6 ± 5.1	41.6 ± 1.6	0.9939	
	PBR(1)	0.42	21.02	171.2 ± 11.5	42.9 ± 3.6	0.9718	

[a] Correlation coefficient of the linear regression analysis.